

Energy Gap Substructures in Conductance Measurements of MgB₂-based Josephson Junctions: Beyond the 2-Gap Model

Steve Carabello,^{1,2,*} Joseph G. Lambert,¹ Jerome Mlack,¹ Wenqing Dai,³ Qi Li,³ Ke Chen,⁴ Daniel Cunnane,⁴ C.G. Zhuang,^{3,4} X. X. Xi,⁴ and Roberto C. Ramos⁵

¹Drexel University, Philadelphia, PA 19104 USA

²Penn State Harrisburg, Middletown, PA 17057, USA

³The Pennsylvania State University, University Park, PA 16802, USA

⁴Temple University, Philadelphia, PA 19122, USA

⁵Indiana Wesleyan University, Marion, IN 46953 USA

(Dated: March 25, 2014)

Several theoretical analyses of the two superconducting energy gaps of magnesium diboride, Δ_π and Δ_σ , predict substructures within each energy gap, rather than two pure numbers. Recent experiments have revealed similar structures. We report tunneling conductance data providing additional experimental evidence for these features. The absence of these features in c -axis tunneling, and a sharp peak in the subgap (associated with the counterelectrode material), support the conclusion that these features are intrinsic to MgB₂. By demonstrating the inadequacy of a simple two-gap model in fitting the data, we illustrate that some distinctions between theoretical models of energy gap substructures are experimentally accessible.

PACS numbers: 74.50.+r, 74.70.Ad, 74.20.-z, 74.25-q

INTRODUCTION

Magnesium diboride (MgB₂) has a number of properties making it a particularly interesting object of study. Among them are its two well-separated energy gaps. Although there had long been both experimental [1, 2] and theoretical [3–5] suggestions of two-gap superconductivity, MgB₂ was the first material to put the matter beyond dispute [6]. Multi-gap superconductivity has recently attracted increased interest, with its demonstration in a variety of materials, including pnictides [7].

As theories were developed for understanding superconductivity in MgB₂, it was recognized that its superconducting energy gap must be both anisotropic and multi-valued: the higher energy gap is associated with the strong σ bonds in the Boron planes, and the lower energy gap is associated with the weaker π bonds.

Several theoretical analyses revealed sub-features in each energy gap, reflecting the electron-phonon interactions in MgB₂. Figure 1(a) shows the Fermi surface of MgB₂ together with the corresponding local density of states at each gap energy [8]. This model was among the earliest to show the distribution in gap energies explicitly. In Figure 1(b), the computed energy gap as a function of energy from the Fermi energy is shown [9]. Near the Fermi level ($\epsilon - E_F = 0$), it also reveals a distribution rather than a single energy, for each gap. A more recent model (Figure 1(c)) [10] also exhibits a distribution in the superconducting gaps of MgB₂. Although each model determines the gap distribution from first principles, differing assumptions and parameter values are applied. These lead to differences in the features of the gap distributions, and the energies at which they appear.

A variety of measurements have provided evidence for

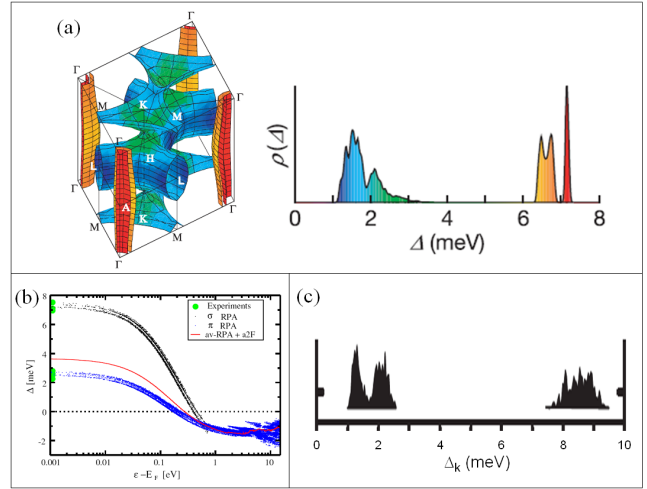


FIG. 1: (color online) Theoretical models for the energy gap distribution of MgB₂. (a) Fermi surface and corresponding gap structure, at $T=0$ (Adapted by permission from Macmillan Publishers Ltd: Nature 418, 758 © 2002 [8]). (b) The superconducting energy gap as a function of energy distance from the Fermi energy at $T = 0$ (reproduced from [9]). (c) Calculated anisotropic superconducting energy gaps, at low temperature (extracted from [10]).

two-gap superconductivity in MgB₂ [6, 11], with conductance curves from tunneling and point-contact spectroscopy proving to be particularly useful techniques [12–16]. As expected, tunneling in the a - b plane shows strong contributions from both the π and σ gaps, while tunneling along the c -axis primarily exhibits the π gap.

Features consistent with substructure within each energy gap have been found in some experimental data [17–21]. These fine features had been thought to be unobserv-

able in physically-realistic systems [22]. Their observation opens a new avenue for exploring superconductivity in MgB_2 .

We have conducted differential conductance measurements on $\text{MgB}_2/\text{I}/\text{Pb}$ and $\text{MgB}_2/\text{I}/\text{Sn}$ junctions with a variety of film geometries. Above T_c of the Pb or Sn electrode, our results are consistent with a simple two-gap model. However, below T_c , our results distinguish simplified two-gap and four-gap models. Therefore, we demonstrate the need to go beyond the two-gap model.

SIMPLE 2-GAP AND 4-GAP THEORY

We begin our analysis with the current-voltage characteristics of a generalized junction between two materials,

$$I(V) = G_n \int_{-\infty}^{\infty} N_1(E) N_2(E + eV) [f(E) - f(E + eV)] dE \quad (1)$$

where G_n is the normal-state conductance of the junction (assumed constant), $N(E)$ is the density of states for each electrode, and $f(E)$ is the Fermi distribution.

Using the BCS density of states for each superconducting electrode,

$$N(E) = \Re \left\{ \sqrt{\frac{E^2}{E^2 - \Delta^2}} \right\} \quad (2)$$

one is able to reproduce the current-voltage characteristics of a basic tunnel junction (neglecting the Josephson supercurrent). Since we measure junctions made from two different electrode materials, each density of states will use a different energy gap Δ_1 and Δ_2 , where Δ_1 (Δ_2) represents the lower (higher) of the two gaps.

In the simplified model we have used (matching that described in [13]), two additional effects are considered:

Broadening Factor Γ : Dynes *et al.* [23] found a broadening in conductance peaks that could not be attributed to temperature. Instead, the quasiparticle lifetime provides a broadening that can be accounted for by replacing all instances of E with $E + i\Gamma$ in the BCS density of states.

Γ has also been used to simulate the effect of a convolution of the theoretical conductance with a distribution of gap values [13]. In this paper, we model the gap distribution as distinct gap energies, with a broadening that phenomenologically matches the experimental gap distribution from our experiments.

Including a constant Γ reveals a feature in the subgap region of the $I - V$ curve, which we have observed and used in our analysis. With a constant Γ included, the modified BCS density of states is nonzero, even at $E = 0$, whether or not the transparency of the junction is zero. This allows the formation of peaks at Δ_1 and Δ_2

in the subgap region, down to $T = 0$, in the absence of Andreev reflections (which require a finite transparency). Because of their strong sensitivity to thermal broadening, the peaks virtually disappear above 3K in theoretical calculations using values similar to those of our junctions. But, the peak at Δ_1 becomes quite sharp as $T \rightarrow 0$.

Weighting for multiple gaps: An additional refinement must be made when considering a multi-gap superconductor. For a two-gap model, a single weighting factor is used:

$$N(E) = w_1 N_1(E) + (1 - w_1) N_2(E) \quad (3)$$

If additional peaks are observed, they can be modeled as additional gaps, each with its own gap energy Δ , its own broadening factor Γ , and its own weight w , as long as the sum of the weights equals 1.

For MgB_2 , two gaps are usually assumed. The weighting factors depend on junction geometry, with $w_\sigma = 1 - w_\pi$ ranging from less than 1% for pure c -axis tunneling, to $\sim 33\%$ for pure a - b plane tunneling [13].

As indicated in Figure 1, two smoothly-broadened gaps (one each for π and σ) may not be sufficient to represent the density of states of MgB_2 . As a result, *within the π (or σ) gap, substructures are necessary, each with its own weighting factor*. For simplicity, we have chosen to model each structure as its own gap, with its own broadening.

From the Fermi surface of MgB_2 , it is evident that the gap value within the π gap will be dependent on the tunneling direction. Therefore, the weights for each substructure should differ for different samples.

We have chosen to compare and contrast our data with a simple 2-gap model (one gap for π and one for σ) vs. a model consisting of four gaps (two each for π and σ). We have observed that, below T_c of the Pb or Sn counter-electrode, a 4-gap model is superior. Above that temperature, 2-gap and 4-gap models cannot be distinguished (see Figure 2).

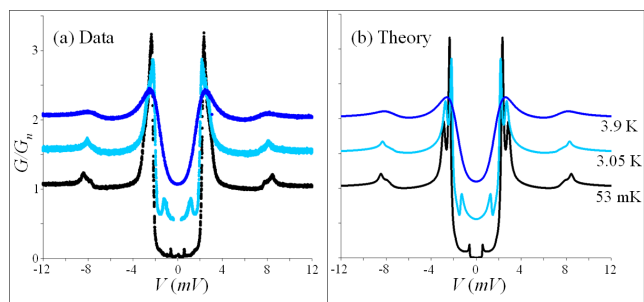


FIG. 2: (color online) (a) Experimental and (b) theoretical normalized conductance vs. voltage curves at 53mK, 3.1K, and 3.9K of an $\text{MgB}_2/\text{I}/\text{Sn}$ junction. Curves have been offset for clarity. The ability to resolve features improves dramatically as the junction transitions from $T > T_{c\text{Sn}}$ (forming an NS junction) to $T < T_{c\text{Sn}} \sim 3.7\text{K}$ (forming an SIS' junction). Above $T_{c\text{Sn}}$, 2-gap and 4-gap models fit the data equally well.

Hereafter, we will refer to these gaps as π_1 , π_2 , σ_1 , and σ_2 , with subscripts 1 (2) referring to the peak at the lower- (higher-) energy sub-peaks of the π and σ gaps. We assume a single sample-dependent gap value Δ , broadening parameter Γ , and weight w for each gap. We emphasize that we are not suggesting a physical source for these gap values. Instead, they serve as a convenient model for the gap distribution.

Neglected Effects: We use a simplified model because we do not assume that any one of the existing theoretical models of the gap distribution is correct. Several additional physical effects have been neglected in our analysis (some of which are described below), either because they have a minor effect on our data, or to limit the number of free parameters to a manageable level.

All of the junctions measured in this study were good tunnel junctions with strong barriers. As a result, there should be little contribution from Andreev reflections, computed using the OBTK model[24–27].

In superconductors with strong electron-phonon coupling, Δ must be treated as a complex function of energy, rather than a constant value. However, theoretical [10, 28, 29] and experimental [30] studies find that their contributions for MgB_2 are small for $|E| \lesssim 30$ meV. We neglect this effect, since our study seeks features within the π and σ gaps ($|E| \leq 15$ meV).

In a two-band superconductor, quasiparticles may scatter from one band to the other, leading to coupled energy-dependent gap functions $\Delta(E)$ [5, 31, 32]. In a two-gap model, this introduces two additional parameters. For a 4-gap model, the number of free parameters would grow unwieldy, without assisting us in our goal of demonstrating the inadequacy of a two-gap model. As a result, we neglect this effect as well.

EXPERIMENTAL DESIGN

Tunneling conductance curves are well-suited for determining the energy gaps and densities of states of superconducting materials. The differential conductance of an N - S junction at $T=0$ is proportional to the density of states of the superconductor; at finite temperature, it is smeared by $\sim \pm 2kT$ [33]. In SIS' junctions, the “very sharply peaked densities of states at the gap edges of both materials helps to counteract the effects of thermal smearing.” [33] (See Figure 2.) By using SIS' junctions at mK temperatures, incorporating extremely high-quality MgB_2 films, we maximize our ability to resolve features within the energy gaps.

For this study, we used $\text{MgB}_2/\text{I}/\text{Pb}$ and $\text{MgB}_2/\text{I}/\text{Sn}$ tunnel junctions incorporating high purity MgB_2 thin films grown by hybrid physical-chemical vapor deposition (HPCVD) on single-crystal SiC substrates[19]. As found by Dai *et al.* [18], on smooth 0° SiC, a largely-planar MgB_2 film forms, exposing primarily the c -axis for tun-

neling. On SiC whose polished surface is tilted 8° from the c -axis, the MgB_2 film takes on a “terraced” shape, exposing the a - b plane. On rough 0° SiC, the growth of the MgB_2 film forms columnar structures, exposing even more of the a - b plane, while still maintaining clean high-quality films. (See Figure 3.)

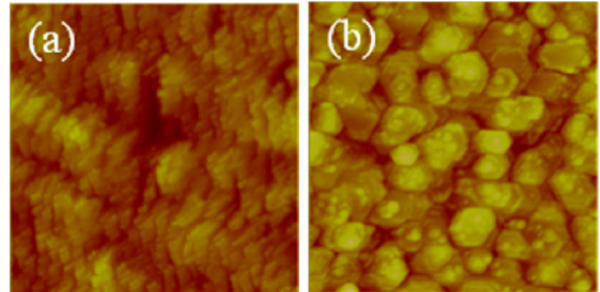


FIG. 3: (color online) AFM images of representative MgB_2 films on SiC (Reprinted with permission from J. Appl. Phys. 113, 083902. Copyright 2013, AIP Publishing LLC. [18]). Each image represents a $2\mu\text{m} \times 2\mu\text{m}$ area. (a) A “terraced” film on 8° SiC, similar to that used for the $\text{MgB}_2/\text{I}/\text{Sn}$ junction discussed below. (b) A “columnar” film on rough c -axis SiC, similar to that used for the $\text{MgB}_2/\text{I}/\text{Pb}$ junction discussed below.

The insulating barrier is formed by a native oxide, which forms upon exposure of the film to air, and creates a good tunnel barrier under proper conditions. A Pb or Sn counterelectrode $\sim 0.3\text{mm}$ wide is then thermally evaporated on a $\sim 0.3\text{mm}$ exposed strip of the film.

These junctions are cooled in a Helium dilution refrigerator with a base temperature $\sim 20\text{mK}$.

The current bias for our junction was provided by sweeping the voltage from an Agilent 3220A function generator, through a bias resistor, prior to reaching the junction. By ensuring $R_{\text{bias}} \gg R_{\text{junction}}$, this combination behaves effectively as a current source. The resulting voltage across the junction was amplified, then recorded. The current bias was swept at between 10 mHz and 1 Hz, while measurements were acquired from 10 kHz to 48 kHz. Such oversampling allows numerical differentiation to produce high-resolution results, by averaging adjacent data points. The number of points in each average was proportional to the time spent near any given voltage. All results were robust under a variety of averaging methods, and a number of results were verified using an SR830 lock-in amplifier, demonstrating that the features are not an artifact of the averaging process.

Electrical isolation of the cryostat was provided by Stanford Research 560 amplifiers operating in differential mode. Additionally, the conductive path through the vacuum pumping lines was broken using plastic clamps and centering rings. High-frequency signals were filtered via thermally-grounded Thermocoax cables, followed by LC and copper powder filters mounted to the cold fin-

ger. Magnetic fields were excluded via cryoperm shielding, and below $\sim 1\text{K}$, the Aluminum sample box expels magnetic fields. Vibration damping pillars supported the cryostat. For most measurements[34], a National Instruments (NI) 9239 DAQ was used to acquire data and store it to the computer. Its inputs are well-isolated, with minimal crosstalk.

Voltage amplification for the “columnar” junction was provided by an SR 560 amplifier operating in differential mode. For the “terraced” and c -axis junctions, a home-built battery-powered amplifier using 4 JFETs in parallel was used.[35, 36] The high input impedance of the JFETs ensures that very little current flows along the voltage measurement lines, and severely limits the ability of noise signals to return to the junction.

KEY RESULTS

Obtaining Δ_{Pb} and Δ_{Sn} from Subgap Features

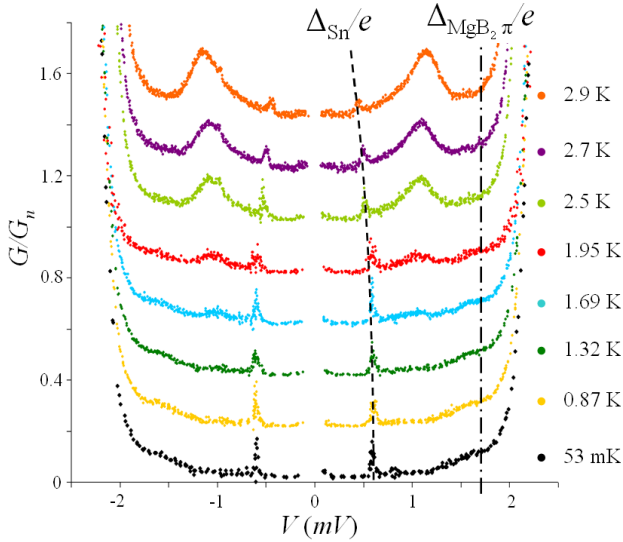


FIG. 4: (color online) Conductance data in the subgap region, for a “terraced” $\text{MgB}_2/\text{I}/\text{Sn}$ junction with $R_n = 15\Omega$ and $R_{sg} \gtrsim 600\Omega$, from 53 mK to 2.9K. Curves have been off-set for clarity. The sharp peak at Δ_{Sn}/e is used to establish Δ_{Sn} in our analysis.

As discussed above, when a nonzero Γ is used, conductance peaks are expected to appear at the gap voltages Δ/e of each superconductor. These are extremely useful, for three reasons. First, they allow us to determine the gap energy of the Pb and Sn counterelectrode to high precision, particularly as $T \rightarrow 0$. Second, because these subgap peaks are sharp and narrow, we are confident that the features we observe in the $(\Delta_{MgB_2} + \Delta_{Sn/Pb})/e$ peaks are due to MgB_2 rather than the counterelectrode material. Finally, they establish that Γ for the counter-

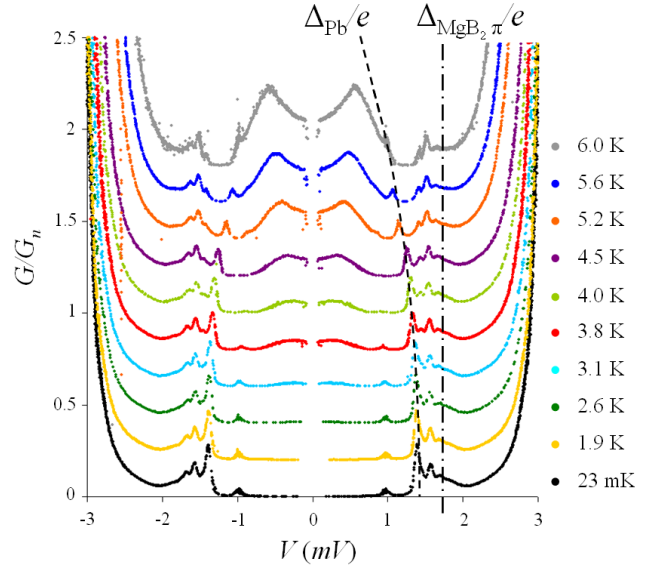


FIG. 5: (color online) Conductance data in the subgap region, for a c -axis $\text{MgB}_2/\text{I}/\text{Pb}$ junction with $R_n = 104\Omega$ and $R_{sg} \gtrsim 13k\Omega$, from 23mK to 6K. The most prominent low-temperature peak appears at Δ_{Pb}/e . The sharpness of this peak, and the small conductance at voltages below this peak, are indications of a small Γ_{Pb} . A broader peak at $\Delta_{MgB_2}\pi/e$ is also evident, exhibiting far less temperature dependence, which is expected for MgB_2 ($T_c = 39\text{K}$). Additional peaks are also evident, which will be discussed in a future article.

electrode material is small, which reduces the parameter space being explored by our models.

Many of the observed features are reasonably consistent with the simple 2-gap (one for π and one for σ) and 4-gap (two each for π and σ) models described above, as can be seen in the subgap portions of Figures 7, 8, and 9. However, a more sophisticated model is required to completely reproduce all of the features. A full discussion is beyond the scope of this paper, and will be addressed in a future article.

We also note that the peak at $\Delta_{MgB_2}\pi/e$ is quite broad, which is appropriate given the distribution in gap values expected in MgB_2 .

At higher T , the peak at $(\Delta_1 - \Delta_2)/e$ appears. This peak is due to quasiparticles thermally excited across the energy gap[33]. The well-defined peaks at both $(\Delta_1 + \Delta_2)/e$ and $(\Delta_1 - \Delta_2)/e$ are widely used to find unique numerical values for both gaps. In this case, however, the $(\Delta_1 - \Delta_2)/e$ peak takes on a rounded appearance due to the distribution in the π gap energies of MgB_2 , in addition to thermal broadening. Therefore, we use the subgap peaks at $\Delta_{Sn/Pb}/e$ together with the peaks at $(\Delta_1 + \Delta_2)/e$ to acquire unique values for each gap.

Calculating Gap Weights

When properly normalized, both theoretical and experimental conductance curves must approach 1 as V approaches infinity. For low-transparency junctions with moderate broadening, it typically becomes quite close to 1 above roughly twice the gap voltage $V_g = (\Delta_1 + \Delta_2)/e$. If a two-gap model is used (one for π and one for σ), then the curve should approach w_π for $eV \gtrsim 2(\Delta_{Pb} + \Delta_\pi)$, and only reach 1 above $(\Delta_{Pb} + \Delta_\sigma)$. If a four-gap model is used (two for π and two for σ), then the curve should approach $(w_{\pi_1} + w_{\pi_2})$ for $eV \gtrsim 2(\Delta_{Pb} + \Delta_{\pi_1})$. Therefore, the weight of the π gap (or the sum of the weights of the π sub-gaps) can be established to good precision, from data; the weight of the σ gap (or the sum of the weights of the σ sub-gaps) will then be $1 - w_\pi$.

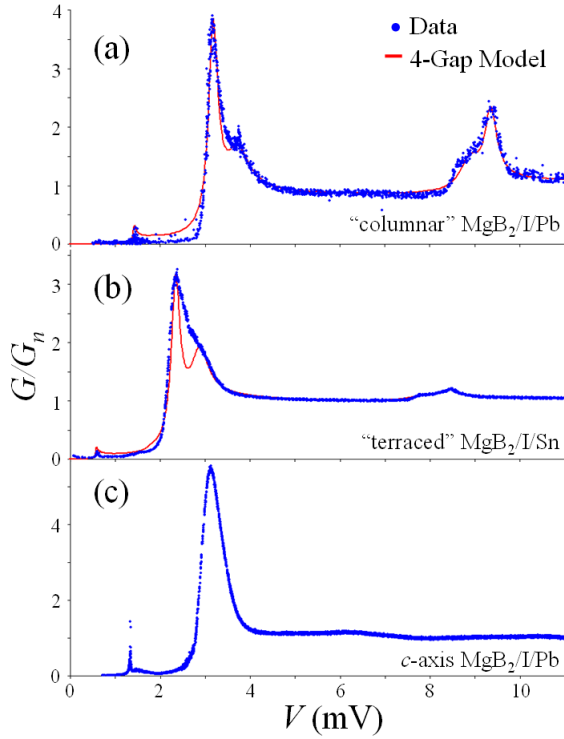


FIG. 6: (color online) Normalized conductance data and models, for two different electrode materials and three film geometries. (a) $\text{MgB}_2/\text{I}/\text{Pb}$ results with a “columnar” MgB_2 film. $w_\sigma \sim 20\%$, indicating significant tunneling along the a - b plane. (b) $\text{MgB}_2/\text{I}/\text{Sn}$ results, with $w_\sigma \sim 6\%$. (c) $\text{MgB}_2/\text{I}/\text{Pb}$ results with a planar “ c -axis” MgB_2 film. The peaks are shifted in voltage due to the difference between the energy gaps of lead ($\Delta_{Pb} \simeq 1.4 \text{ meV}$) and tin ($\Delta_{Sn} \simeq 0.57 \text{ meV}$). The “shelf” feature at $\sim 7 \text{ mV}$ in the $\text{MgB}_2/\text{I}/\text{Pb}$ data, and one at $\sim 11 \text{ mV}$ (not shown), are associated with peaks in the Eliashberg spectral function $\alpha^2 F(E)$ of the strongly-coupled superconductor Pb.[37]

Applying this method to our “columnar” $\text{MgB}_2/\text{I}/\text{Pb}$ junction, we find $w_\sigma \simeq 20\%$. This value is remarkably high, considering that the MgB_2 film was deposited on

0° SiC, and the theoretical maximum for pure a - b plane tunneling is $\sim 33\%$. The “terraced” $\text{MgB}_2/\text{I}/\text{Pb}$ junction we studied has $w_\sigma \sim 6\%$. And, as expected, for tunneling to a pure c -axis MgB_2 film, the σ peak was indistinguishable ($w_\sigma < 1\%$).

π Gap Substructure

A majority of Cooper pairs tunneling into an MgB_2 surface are expected to tunnel to the π gap. However, the precise details will be sample-dependent. Here, we consider the three significantly different film geometries described above.

“**Columnar**”: On a rough 0° SiC substrate, an MgB_2 film was grown, which formed columnar structures (Figure 3 (b)). Pb was thermally evaporated as the counter-electrode. Since the MgB_2 crystallites were far smaller than the area of Pb in contact with the film, tunneling could occur along the c -axis, along the a - b plane, and anywhere in between. This allows the entire Fermi surface to be explored simultaneously.

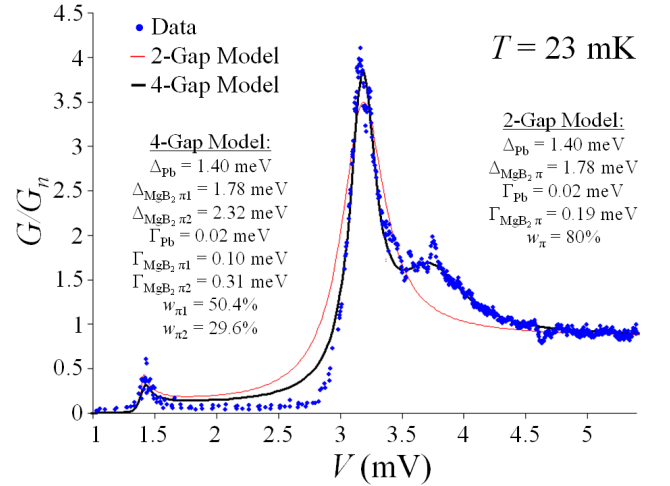


FIG. 7: (color online) Normalized conductance, showing the π gap for the $\text{MgB}_2/\text{I}/\text{Pb}$ “columnar” junction. This data is well-modeled using two π gaps at 1.78 and 2.32 meV (with additional gaps for sigma), while a single π peak is unable to capture significant portions of the data.

The gap distributions shown in Figure 1(a) and (c)[8, 10] suggest that the π gap has a double-peaked structure. Low-temperature data for this “columnar” sample, shown in Figure 7, as predicted, displays a double peak at the gap voltage $(\Delta_{\text{MgB}_2\pi} + \Delta_{Pb})/e$.

Clearly, a model possessing a single π gap cannot reproduce this structure. However, a simple model reflecting features for both π_1 and π_2 (in addition to multiple σ gaps, described below) produces remarkable agreement.

The peak in the subgap region establishes Δ_{Pb} , while the level of the normalized conductance between

$\sim 5\text{mV}$ and $\sim 8\text{mV}$ establishes w_π in a 2-gap model, or $(w_{\pi_1} + w_{\pi_2})$ in a 4-gap model. Using the taller peak at $(\Delta_{\pi_1} + \Delta_{Pb})/e$, $\Delta_{MgB_2\pi_1}$ was determined to a high precision: 1.78meV with an uncertainty of $\pm 0.02\text{meV}$. (All uncertainties are estimated by finding a range of parameters that produce reasonable fits, similar to the method outlined in [13].)

The remaining parameters in the 4-gap model are less certain. Given the asymmetry of the π_2 shoulder, reasonably good 4-gap fits yield $\Delta_{MgB_2\pi_2}$ of 2.32meV with an uncertainty of $\sim \pm 0.1\text{meV}$. The weights w and the broadening parameters Γ are more uncertain, because according to the model, any peak may have its height decreased by increasing Γ or by decreasing w , and vice versa. However, as seen in Figure 1, there are not two simple sharp peaks for the π gap; and the broadening parameter is here being used exclusively as a means of approximating a distribution in the gap energies. So, although w and Γ necessary parameters in the fit, they do not affect our goal in establishing the need for more than a single broadened π gap.

Therefore, we have demonstrated that a single gap energy for the π gap is quite far from the real behavior of MgB_2 , while a π gap possessing two distinct sub-bands is a reasonable approximation.

“Terraced”: The $MgB_2/I/Sn$ “terraced” junction used an MgB_2 film formed of parallel tilted layers, each exposing a portion of the a - b plane as well as the c -axis.

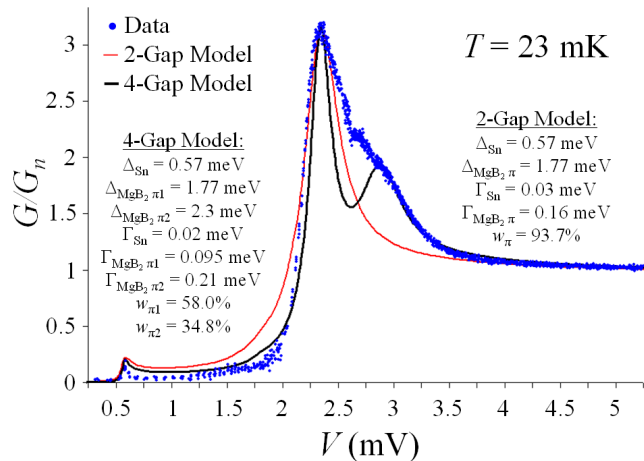


FIG. 8: (color online) π gap for the $MgB_2/I/Sn$ “terraced” junction. The prominent shoulder at $\sim 3\text{mV}$ indicates that a single gap energy is not appropriate for the π gap. A better fit is given by a four-gap model with π gap values of $\pi_1 = 1.77\text{meV}$ and $\pi_2 = 2.3 \text{ meV}$.

Once again, a single π gap model fits this data very poorly. As shown in Figure 8, our simple model including π_1 and π_2 is less successful than for the “columnar” sample, though it still does capture some of the main features. Here, fitting to the tallest peak yields a π_1 gap voltage of $1.77 \pm 0.04 \text{ meV}$. However, the broad shoulder

can be fit by a wide range of π_2 gap energies, with an uncertainty of $\sim \pm 0.2\text{meV}$.

Within our model, it was not possible to faithfully fit the data, as shown in Figure 8. This suggests that a more sophisticated model, capable of accounting for additional sample-dependent effects, is required. However, we have demonstrated that a single π gap, no matter how much it is broadened, is inconsistent with the data.

c – axis: In pure c -axis tunneling, almost all of the tunneling is to the π gap, with minimal contribution from the σ gap. Moreover, the distribution within the π gap should be more limited than in cases where the a - b plane is exposed, since less of the Fermi surface is being explored.

Low-temperature data on a c -axis $MgB_2/I/Pb$ junction is shown in Figure 9. It consists mainly of a single peak, centered at the lower-energy π_1 sub-gap. (That is, the peak appears at a voltage $(\Delta_{MgB_2\pi_1} + \Delta_{Pb})/e$.) However, using a single-gap theory with variable Γ , it was not possible to find a combination of Δ and Γ which make the peak broad enough to match the data.

From this data alone, it is not clear whether a distribution in gap energies is required, or if a different broadening (which cannot be modeled using Γ) is sufficient.

However, we gain increased confidence in the significance of features observed in the other film geometries because, as expected, this junction shows a more limited distribution. Each film was fabricated using similar methods, and all were deposited on SiC. So, it is reasonable to expect that any artificial contributions due to variations in film strain or other effects should have appeared in these c -axis samples as well. That they did not supports our suggestion that they are inherent properties of MgB_2 .

σ Gap Substructure

The high T_c of MgB_2 is due to the Cooper pairs forming in the σ band. Therefore, understanding the σ gap is of key importance in theoretical models. As shown in Figure 1, there are appreciable differences between different models, so high-resolution gap measurements may be of value.

As seen in Figure 6(c), tunneling to a c -axis MgB_2 surface naturally shows no features in the σ gap. However, the other contact geometries do produce useful information.

The “columnar” $MgB_2/I/Pb$ junction data exhibits features that are clearly incompatible with a simple 2-gap model. If there is only a single σ gap, then the resulting curve must take on the shape of a broadened BCS density of states: a steeper low-energy edge, and a gradual decay toward its limiting value of 1 at higher energies. Our data reveals exactly the opposite: a relatively sharp peak at high energies, together with a prominent lower-energy

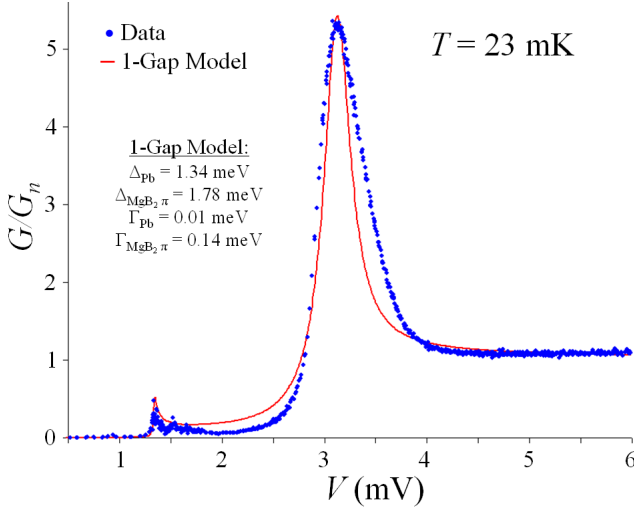


FIG. 9: (color online) π gap for a $\text{MgB}_2/\text{I}/\text{Pb}$ c-axis junction. With tunneling purely along the c-axis of MgB_2 , far less of the Fermi surface is being explored. As a result, the gap distribution is far less apparent. Even so, a single π gap (broadened via Γ) is unable to match the data.

shoulder. These features are reasonably well-modeled by two separate σ gaps (which, together with the two π gaps form a 4-gap model). However, there are some features that cannot be fit by two sub-gaps within σ . Indeed, the theoretical models shown Figure 1 suggest that two peaks are insufficient to accurately portray the σ gap.

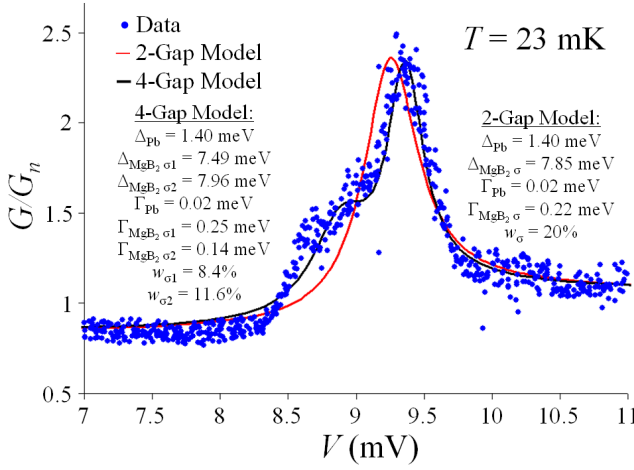


FIG. 10: (color online) σ gap for the $\text{MgB}_2/\text{I}/\text{Pb}$ “columnar” junction. A series of features, including a prominent shoulder at a lower voltage than the main peak, indicate that the σ gap is more complex than a single broadened peak.

The “terraced” $\text{MgB}_2/\text{I}/\text{Sn}$ junction also exhibits a sharper peak at higher energies, and a prominent lower-energy shoulder. However, since w_σ is $\sim 6\%$ (in contrast to the “columnar” junction’s $\sim 20\%$), the peaks are less pronounced. As shown in Figure 11, a single σ gap is far from adequate for representing this data, while two σ

sub-peaks models the data reasonably well.

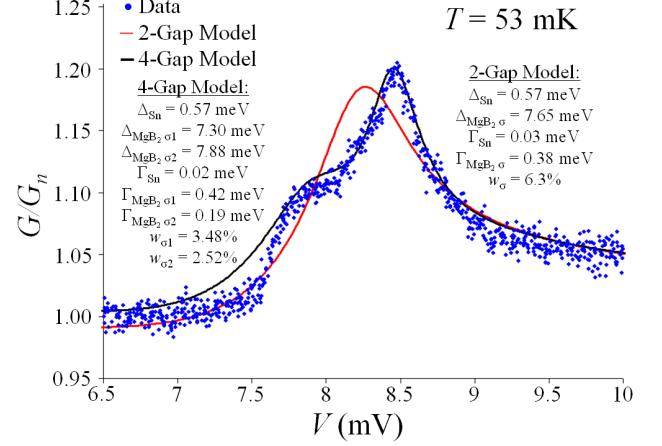


FIG. 11: (color online) σ gap for the $\text{MgB}_2/\text{I}/\text{Sn}$ “terraced” junction. As above, a prominent shoulder appears at a voltage below that of the main peak.

DISCUSSION

We have summarized our results in Table I. Our data shows that our experiments can resolve features down to less than 0.5meV apart. As noted earlier, features in NS conductance data are expected to be thermally smeared by $\sim 2k_B T$. This corresponds to 0.69meV at 4K , and 0.17meV at 1K . SIS' conductance data should be even sharper. This suggests our results are not thermally limited.

Scattering will also limit the ability to resolve features within the energy gaps. The scattering rate γ may be calculated from $\gamma > \sqrt{\langle \Delta \rangle \delta \Delta}$ [22], where $\langle \Delta \rangle$ is the average order parameter, and $\delta \Delta$ is the variation of the order parameter over the Fermi surface. If we equate these with the average energy gap value and the resolution of our energy gap data, respectively, we find a scattering rate on the order of 1 meV . This implies a mean free path beyond 300 nm . Since this distance is on the same order as irregularities in the film surface ([18]), it is surprising to observe this energy gap substructure, even with extremely clean samples. Nevertheless, prior tunneling spectroscopy experiments at temperatures from 7.0K to 1.8K have exhibited such resolved features[17, 18], in addition to our experimental results presented here.

Table I also illustrates a significant discrepancy between our experimental results and those from theory (a): our energy gap values are consistently $\sim 10\%$ higher. There are several reasonable explanations for this.

Nearly half of this difference may be accounted for by considering the effect of strain (caused by different thermal expansion coefficients, as the sample is cooled after growing the film) on energy gaps. It has been found

TABLE I: Comparison of energy gap values of MgB_2 derived from fits to experimental data vs. peaks in theoretical density of states calculations. Experimental uncertainties are estimated by the range of gap values for which a 4-gap fit may produce reasonable agreement with the data. Theoretical values are based on the center of each peak. Values for Δ_σ for Theory (c) are approximate, as it is not easily separated into two sub-peaks.

Feature	“Columnar” Data	“Terraced” Data	Theory (a) [8]	Theory (c) [10]
$\Delta_{\pi 1}$ (meV)	1.78 ± 0.02	1.77 ± 0.04	1.51	1.3
$\Delta_{\pi 2}$ (meV)	2.32 ± 0.1	2.3 ± 0.2	2.06	2.2
$\Delta_{\sigma 1}$ (meV)	7.49 ± 0.3	7.30 ± 0.2	6.61	~ 8.2
$\Delta_{\sigma 2}$ (meV)	7.96 ± 0.05	7.88 ± 0.05	7.13	~ 8.7

experimentally [38] that T_c is approximately 41.5K for MgB_2 films on SiC, rather than the conventional value of 39.4K.

A key prediction of BCS theory is the value of the energy gap at zero temperature [33]:

$$E_g(0) = 2\Delta(0) = 3.528k_B T_c \quad (4)$$

Therefore, elevating T_c from 39.4K to 41.5K provides a roughly 5.3% increase in the energy gap values. Similar experiments using similar samples also found the sigma gap significantly elevated when using SiC as the substrate for the MgB_2 film, rather than MgO (which has a much smaller mismatch in expansion coefficients) [17, 18].

The remaining discrepancy may be due to using thin films for the experimental realization of this measurement, rather than the periodic boundary conditions used in calculations. Additional systematic differences between experiment and theory are known to exist.

CONCLUSION

We have performed high-resolution tunneling measurements of low-transparency MgB_2 tunnel junctions using “terraced,” “columnar,” and *c*-axis geometries, at low (4K) to very low (23 mK) temperatures. With these measurements, we have probed the substructures within the π and σ gaps of MgB_2 .

Within the subgap, we observed very sharp peaks that identify, to high precision, the values of the energy gaps of the junction counterelectrodes (Pb and Sn). These lead us to conclude that the substructures seen in the π and σ gaps are due to MgB_2 , consistent with prior reported measurements [17–21].

Using a simplified two-band and four-band model with variable gap weights and broadening factors, we demonstrate how these sub-structures illustrate the need to go beyond a two gap model.

This research has been supported by a grant in aid from Sigma Xi, the Scientific Research Society.

R.C.R. acknowledges partial support from National Science Foundation Grant # DMF-1206561 and Q.L. acknowledges support from DOE DE-FG02-08ER46531

(Q.L.). The work at Temple University was supported by ONR under Grant No. N00014-13-1-0052.

* Electronic address: sac69@drexel.edu

- [1] J. W. Hafstrom and M. L. A. MacVicar, Phys. Rev. B **2**, 4511 (1970), URL <http://link.aps.org/doi/10.1103/PhysRevB.2.4511>.
- [2] B. L. Blackford, Phys. Rev. B **5**, 1171 (1972), URL <http://link.aps.org/doi/10.1103/PhysRevB.5.1171>.
- [3] H. Suhl, B. T. Matthias, and L. R. Walker, Phys. Rev. Lett. **3**, 552 (1959), URL <http://link.aps.org/doi/10.1103/PhysRevLett.3.552>.
- [4] D. Rogovin and M. Scully, Phys. Rep. **25**, 175 (1976), URL <http://www.sciencedirect.com/science/article/pii/00370157376900119>.
- [5] N. Schopohl and K. Scharnberg, Solid State Commun. **22**, 371 (1977), ISSN 0038-1098, URL <http://www.sciencedirect.com/science/article/pii/0038109877910699>.
- [6] X. X. Xi, Rep. Prog. Phys. **71**, 116501 (2008), URL <http://stacks.iop.org/0034-4885/71/i=11/a=116501>.
- [7] P. Seidel, Superconductor Science and Technology **24**, 043001 (2011), URL <http://stacks.iop.org/0953-2048/24/i=4/a=043001>.
- [8] H. J. Choi, D. Roundy, H. Sun, M. L. Cohen, and S. G. Louie, Nature **418**, 758 (2002).
- [9] A. Floris, G. Profeta, N. N. Lathiotakis, M. Lüders, M. A. L. Marques, C. Franchini, E. K. U. Gross, A. Continenza, and S. Massidda, Phys. Rev. Lett. **94**, 037004 (2005), URL <http://link.aps.org/doi/10.1103/PhysRevLett.94.037004>.
- [10] E. R. Margine and F. Giustino, Phys. Rev. B **87**, 024505 (2013), URL <http://link.aps.org/doi/10.1103/PhysRevB.87.024505>.
- [11] X. K. Chen, M. J. Konstantinović, J. C. Irwin, D. D. Lawrie, and J. P. Franck, Phys. Rev. Lett. **87**, 157002 (2001), URL <http://link.aps.org/doi/10.1103/PhysRevLett.87.157002>.
- [12] M. Iavarone, G. Karapetrov, A. E. Koshelev, W. K. Kwok, G. W. Crabtree, D. G. Hinks, W. N. Kang, E.-M. Choi, H. J. Kim, H.-J. Kim, et al., Phys. Rev. Lett. **89**, 187002 (2002), URL <http://link.aps.org/doi/10.1103/PhysRevLett.89.187002>.
- [13] D. Daghero and R. S. Gonnelli, Supercon. Sci. Technol. **23**, 043001 (2010), URL <http://stacks.iop.org/0953-2048/23/i=4/a=043001>.

- [14] R. S. Gonnelli, D. Daghero, G. A. Ummarino, V. A. Stepanov, J. Jun, S. M. Kazakov, and J. Karpinski, *Phys. Rev. Lett.* **89**, 247004 (2002), URL <http://link.aps.org/doi/10.1103/PhysRevLett.89.247004>.
- [15] Y. Ponomarev, S. Kuzmichev, M. Mikheev, M. Sudakova, S. Tchesnokov, N. Timergaleev, A. Yargin, E. Maksimov, S. Krasnosvobodtsev, A. Varlashkin, et al., *Solid State Commun.* **129**, 85 (2004), ISSN 0038-1098, URL <http://www.sciencedirect.com/science/article/pii/S0038109803008573>.
- [16] H. Schmidt, J. Zasadzinski, K. Gray, and D. Hinks, *Physica C* **385**, 221 (2003), ISSN 0921-4534, URL <http://www.sciencedirect.com/science/article/pii/S0921453402023171>.
- [17] K. Chen, W. Dai, C. Zhuang, Q. Li, S. Carabello, J. G. Lambert, J. T. Mlack, R. C. Ramos, and X. X. Xi, *Nat. Commun.* **3**, 619 (2012), URL <http://dx.doi.org/10.1038/ncomms1626>.
- [18] W. Dai, K. Chen, X. X. Xi, and Q. Li, *J. Appl. Phys.* **113** (2013), ISSN 0021-8979.
- [19] K. Chen, Y. Cui, Q. Li, C. G. Zhuang, Z.-K. Liu, and X. X. Xi, *Appl. Phys. Lett.* **93**, 012502 (pages 3) (2008), URL <http://link.aip.org/link/?APL/93/012502/1>.
- [20] Y. Ponomarev, S. Kuzmichev, N. Kadomtseva, M. Mikheev, M. Sudakova, S. Chesnokov, E. Maksimov, S. Krasnosvobodtsev, L. Sevastyanova, K. Burdina, et al., *JETP Lett.* **79**, 484 (2004), ISSN 0021-3640, URL <http://dx.doi.org/10.1134/1.1780557>.
- [21] S. Carabello, J. Lambert, J. Mlack, and R. Ramos, *IEEE Trans. Appl. Supercond.*, **21**, 3083 (2011), ISSN 1051-8223.
- [22] I. I. Mazin, O. K. Andersen, O. Jepsen, A. A. Golubov, O. V. Dolgov, and J. Kortus, *Phys. Rev. B* **69**, 056501 (2004).
- [23] R. C. Dynes, V. Narayanamurti, and J. P. Garno, *Phys. Rev. Lett.* **41**, 1509 (1978), URL <http://link.aps.org/doi/10.1103/PhysRevLett.41.1509>.
- [24] M. Octavio, M. Tinkham, G. E. Blonder, and T. M. Klapwijk, *Phys. Rev. B* **27**, 6739 (1983), URL <http://link.aps.org/doi/10.1103/PhysRevB.27.6739>.
- [25] K. Flensberg, J. B. Hansen, and M. Octavio, *Phys. Rev. B* **38**, 8707 (1988), URL <http://link.aps.org/doi/10.1103/PhysRevB.38.8707>.
- [26] M. Hurd, S. Datta, and P. F. Bagwell, *Phys. Rev. B* **54**, 6557 (1996), URL <http://link.aps.org/doi/10.1103/PhysRevB.54.6557>.
- [27] M. Hurd, S. Datta, and P. F. Bagwell, *Phys. Rev. B* **56**, 11232 (1997), URL <http://link.aps.org/doi/10.1103/PhysRevB.56.11232>.
- [28] O. V. Dolgov, R. S. Gonnelli, G. A. Ummarino, A. A. Golubov, S. V. Shulga, and J. Kortus, *Phys. Rev. B* **68**, 132503 (2003), URL <http://link.aps.org/doi/10.1103/PhysRevB.68.132503>.
- [29] I. K. Yanson, S. I. Beloborod'ko, Y. G. Naidyuk, O. V. Dolgov, and A. A. Golubov, *Phys. Rev. B* **69**, 100501 (2004), URL <http://link.aps.org/doi/10.1103/PhysRevB.69.100501>.
- [30] J. Geerk, R. Schneider, G. Linker, A. G. Zaitsev, R. Heid, K.-P. Bohnen, and H. v. Löhneysen, *Phys. Rev. Lett.* **94**, 227005 (2005), URL <http://link.aps.org/doi/10.1103/PhysRevLett.94.227005>.
- [31] Y. Noat, T. Cren, F. Debontridder, D. Roditchev, W. Sacks, P. Toulemonde, and A. San Miguel, *Phys. Rev. B* **82**, 014531 (2010), URL <http://link.aps.org/doi/10.1103/PhysRevB.82.014531>.
- [32] Y. Noat, T. Cren, P. Toulemonde, A. San Miguel, F. Debontridder, V. Dubost, and D. Roditchev, *Phys. Rev. B* **81**, 104522 (2010), URL <http://link.aps.org/doi/10.1103/PhysRevB.81.104522>.
- [33] M. Tinkham, *Introduction to Superconductivity: Second Edition* (Dover Publications, 1996), ISBN 0486435032.
- [34] For the MgB₂/I/Pb “columnar” junction, a NI 9215 DAQ was used. Its ports are not isolated; therefore, more averaging was necessary —though still reasonable considering the degree of oversampling.
- [35] H. Xu, Ph.D. thesis, University of Maryland at College Park (2004).
- [36] A. J. Berkley, Ph.D. thesis, University of Maryland at College Park (2003).
- [37] E. Wolf, *Principles of Electron Tunneling Spectroscopy: Second Edition*, International Series of Monographs on Physics (OUP Oxford, 2011), ISBN 9780191628160.
- [38] A. V. Pogrebnyakov, J. M. Redwing, S. Raghavan, V. Vaithyanathan, D. G. Schlom, S. Y. Xu, Q. Li, D. A. Tenne, A. Soukiassian, X. X. Xi, et al., *Phys. Rev. Lett.* **93**, 147006 (2004).